PAPER

Near-circularly polarized single attosecond pulse generation from nitrogen molecules in spatially inhomogeneous laser fields

IOP Publishing Journal of Physics B: Atomic, Molecular and Optical Physics
J. Phys. B: At. Mol. Opt. Phys. **49** (2016) 015602 (11pp) doi:10.1088/0953-4075/49/1/015602

Near-circularly polarized single attosecond pulse generation from nitrogen molecules in spatially inhomogeneous laser fields

Xiaofan Zhang[1], Yang Li[1], Xiaosong Zhu[1], Qingbin Zhang[1], Pengfei Lan[1] and Peixiang Lu[1,2]

[1] School of Physics and Wuhan National Laboratory for Optoelectronics, Huazhong University of Science and Technology, Wuhan 430074, People's Republic of China
[2] Laboratory of Optical Information Technology, Wuhan Institute of Technology, Wuhan 430073, People's Republic of China

E-mail: zhuxiaosong@hust.edu.cn and pengfeilan@hust.edu.cn

Received 7 September 2015
Accepted for publication 6 November 2015
Published 4 December 2015

Abstract

The generation of an attosecond pulse in nitrogen molecules using spatially inhomogeneous laser fields is investigated by numerically solving the time-dependent Schrödinger equation. It is found that an isolated attosecond pulse with elliptical polarization can be generated using linearly polarized laser fields. By changing polarization direction with respect to the molecular axis, the ellipticity of the attosecond pulse can be easily controlled. At some specific angles, the intensities of the two mutually vertical harmonic components, parallel and perpendicular to the driving laser polarization direction, are comparable. Additionally, the relative phase between the two components is about $\pi/2$. As a result, it supports the generation of the isolated near-circularly polarized attosecond pulse with a duration of 155 as.

Keywords: high harmonic generation, spatially inhomogeneous laser fields, isolated near-circularly polarized attosecond pulse

(Some figures may appear in colour only in the online journal)

1. Introduction

High-order harmonic generation (HHG) is a highly nonlinear phenomenon in strong field light-matter interactions. In the past two decades, HHG has been intensively investigated for its potential applications in experimentally generating a coherent attosecond pulse [1, 2] in the extreme ultraviolet (XUV) and soft x-ray regions [3]. The availability of isolated attosecond pulses has successfully opened new research areas for probing ultrafast processes of physics, chemistry and biology with unprecedented temporal and spatial resolutions [4–11]. For example, it has been shown that an attosecond XUV pulse can be used to study inner-shell electron dynamics in atoms and molecules [12, 13].

The mechanism of the HHG can be well described by the classical three-step model (CTSM) [14]: ionization, acceleration, and recombination. The CTSM not only provides a clear physical picture of HHG, but also suggests that the HHG process can be controlled by modulating different steps to generate intense isolated attosecond pulses. Many different schemes have been proposed for this purpose, including using a few-cycle laser pulse [15–17], the polarization gating technique [2, 18–21], two-color (or multi-color) control schemes [17, 22–26] and, more recently, using plasma-enhanced inhomogeneous laser fields [27–33].

Most previous considerations have concentrated on the generation of linearly polarized attosecond pulses [6, 24]. In the applications, the elliptical polarization characteristic of an isolated attosecond pulse, which provides an additional degree of freedom, is also very important. For example, Mairesse *et al* [34] demonstrated that elliptically polarized harmonics can be applied in the harmonics spectroscopy of oriented N_2 to track multichannel dynamics during strong-field ionization. The developments of circularly polarized

attosecond pulses thus make it possible to create spinning circular electron wave packets, leading to large time-dependent internal magnetic fields in matter on the attosecond time scale [35]. Optically induced ultrafast magnetization reversal has now been reported, by circularly polarized pulses in material science [36], thus emphasizing new and further applications of such pulses.

Recently, some methods have been also proposed for single circularly polarized attosecond pulse generation. Near-circularly polarized high harmonics and attosecond pulses have been theoretically investigated by using ring-current states with angular momentum of up to $|m| = 6$ [37]. The bichromatic circularly polarized laser fields with opposite rotation polarization directions can also be used for the circularly polarized HHG [38, 39]. Yuan *et al* have shown that circularly polarized high-order harmonics can be generated by the combination of an elliptically polarized laser and strong static fields in molecular ions [35, 40] or the few-cycle elliptically polarized laser pulse and terahertz fields from molecular media [41]. But these methods have limitations in that the recombination probability drops significantly as the driving laser ellipticity increases. So the efficiency of HHG is much lower than that with a linearly polarized laser field [42]. In contrast, using a linearly polarized laser field has been experimentally and theoretically recognized as a promising route to increase efficiency [43–46]. However, the time duration of the attosecond pulse is made relatively long by implementing all these methods above, and therefore shorter circularly polarized pulses are highly desired.

In this paper, we propose an effective method to generate short near-circularly polarized isolated attosecond pulses with high efficiency in nitrogen molecules using a linearly polarized inhomogeneous laser field in the vicinity of metallic nanostructures. We have found that the intensities of the two mutually vertical polarized harmonic components are comparable and the relative phase is $\pi/2$ at specific alignment angles, thus the high-order harmonics generated exhibit large ellipticity as high as 0.97. Besides, a broadband supercontinuum appears in the harmonic spectrum, which is due to the spatial inhomogeneity of the plasma-enhanced laser field [47–49]. The amplitudes of the electrons in the continuum present an excessive excursion [50] in the inhomogeneous field such that the the cutoff of the harmonic is significantly extended. The broad bandwidth together with the large ellipticity of the supercontinuum makes it possible to efficiently generate intense isolated near circularly polarized attosecond pulses with a duration of 155 as.

2. Theoretical model

Numerically computing the high-order harmonic spectrum generated from the interaction between a linearly polarized spatially inhomogeneous laser field and N_2 molecules is based on the two-dimensional time-dependent Schrödinger equation, which can be written as (atomic units (a.u.) are used throughout this paper) [51]

$$\mathrm{i}\frac{\partial\Psi(\vec{r},t)}{\partial t} = H(\vec{r},t)\Psi(\vec{r},t). \tag{1}$$

$H(\vec{r},t)$ is the Hamilton given by

$$H(\vec{r},t) = -\frac{1}{2}\nabla^2 + V(\vec{r}) - xE(x,t), \tag{2}$$

in which x is the polarization direction of the laser pulse. To correctly reproduce the HOMO of N_2 molecules, we use a soft core potential [52], which has the form

$$V(\vec{r}) = \sum_{\alpha=1}^{2}\frac{-Z_\alpha(\vec{r_\alpha})}{\sqrt{|\vec{r_\alpha}|^2 + a_\alpha^2}}. \tag{3}$$

The position-dependent effective charge is

$$Z_\alpha(\vec{r}) = Z_\alpha^\infty + (Z_\alpha^0 - Z_\alpha^\infty)\exp\left[-\frac{|\vec{r} - \vec{\rho_\alpha}|^2}{\sigma_\alpha^2}\right]. \tag{4}$$

$\alpha = 1,\ 2$ labels the nuclei at fixed positions $\vec{\rho_\alpha}$ and $\vec{r_\alpha} = \vec{r} - \vec{\rho_\alpha}$ where $\vec{r} \equiv (x, y)$ denotes the electron position in the two-dimensional x-y plane. The soft Coulomb potential parameter a_α is chosen to be 1.2, and $Z_\alpha^\infty = 0.500$ denotes the effective nuclear charge of the nucleus α as seen by an electron at infinite distance. Similarly, $Z_\alpha^0 = 7$ is the bare charge of nucleus α. The value of $\sigma_\alpha = 0.700$ represents the degree of attenuation of the effective charge of the nucleus with distance and is introduced to account for distance-dependent electron-electron screening effects.

The spatially inhomogeneous field can be represented in the following form [53]

$$E(x,t) = E_0(1 + \kappa x)f(t)\cos(\omega t + \phi), \tag{5}$$

where κ determines the spatial inhomogeneity strength of the plasmonic electric field and its unit is in the reciprocal length. We choose 1600 nm as the driving laser wavelength. ω and ϕ represent respectively the angular frequency and the carrier envelope phase (CEP) of the driving field. $E_0 = 0.0925$ a.u. is the amplitude of the electric field, corresponding to the peak intensity of 3×10^{14} W·cm^{-2}. It is worth emphasizing that this intensity is not the initial input laser intensity but the plasmonic enhanced intensity in the hot spot. A sin-squared envelope $\sin^2\left(\frac{\pi t}{T}\right)$ is used to characterize the pulse profiles f(t) in which we set $T = 3T_0$ and T_0 denotes the optical cycle of the driving laser pulse. And the full width at half maximum (FWHM) of the driving pulse is about 6 fs.

We use the split-operator method to solve equation (1) [51]. To avoid spurious reflections from the spatial boundaries, the electron wave function $\Psi(\vec{r},t)$ is multiplied by a 'mask function' $g(t)$ with the following form [54]

$$g(t) = g_x(t)g_y(t) \tag{6}$$

at each time step, in which

$$g_x(t) = \begin{cases} 1 & |x| < R_x - L_x \\ \sin^{1/8}\left(\frac{R_x - |x|}{2\pi L_x}\right) & |x| \geqslant R_x - L_x \end{cases} \tag{7}$$

and

$$g_y(t) = \begin{cases} 1 & |y| < R_y - L_y \\ \sin^{1/8}\left(\frac{R_y - |y|}{2\pi L_y}\right) & |y| \geqslant R_y - L_y \end{cases}. \quad (8)$$

For all results reported here, we set the 'absorber' domain of the two directions $L_x = 20$ a.u. and $L_y = 20$ a.u., $R_x = R_y = 100$ a.u. In our calculation, we set the range of the 'mask function' from -100 a.u. to 100 a.u. in the Cartesian coordinates. The space step is 0.1 a.u.. The time step is $\Delta t = 0.05$ a.u.. The time-dependent dipole acceleration can be calculated by means of the Ehrenfest theorem

$$A_q(t) = -\langle \Psi(t)|[H(t), [H(t), q]]|\Psi(t)\rangle, q = x, y. \quad (9)$$

Then, the harmonic spectrum is obtained by Fourier transforming the dipole acceleration

$$a_q(\omega) = \int A_q(t)\exp(-iq\omega t)dt, \quad (10)$$

$$D_q = \left|a_q(\omega)\right|^2, \quad (11)$$

and the attosecond pulse generated from high-order harmonics can be obtained by inverse Fourier transformation of the harmonic

$$I_q = \left| \int a_q(\omega)\exp(iq\omega t)dt \right|^2. \quad (12)$$

The amplitude ratio and the phase difference between the two orthogonal harmonic components are calculated by $R = \frac{|a_q^y|}{|a_q^x|}$ and $\delta = \arg\left[a_q^y\right] - \arg\left[a_q^x\right]$ respectively. $a_q^x a_q^y$ are the two perpendicular components of $a_q\omega$, and the ellipticity is finally obtained by the following formula [55]:

$$\varepsilon = \sqrt{\frac{1 + R^2 - \sqrt{1 + 2R^2\cos(2\delta) + R^4}}{1 + R^2 + \sqrt{1 + 2R^2\cos(2\delta) + R^4}}}. \quad (13)$$

When $R = 0$ or $\delta = 0$ or π, the ellipticity $\varepsilon = 0$ and the harmonic is linearly polarized, otherwise it will be elliptically or circularly polarized. In this work, our purpose is to obtain an attosecond pulse with the maximum ellipticity.

3. Results and discussions

Firstly, a sketch of our coordinate systems is presented in figure 1, where (x', y', z') is the molecule frame and (x, y, z) is the laboratory frame. In the bottom right hand corner of figure 1, the incident laser linearly polarizes along the x-axis and its propagation direction is along the z-axis. The angle between the laser polarization direction and molecular axis is denoted as β. Without the use of chirped pulse amplification (CPA), the output power of a moderate femtosecond oscillator will locate in the range 10^{11}–10^{12} W · cm^{-2} [48], which can not support the HHG. The metallic nanostructure (e.g., the gold bow-tie shaped nanostructures [56]), by exploiting surface plasmon resonances [57], offers an efficient way to enhance the incident laser field to reach the intensity level for

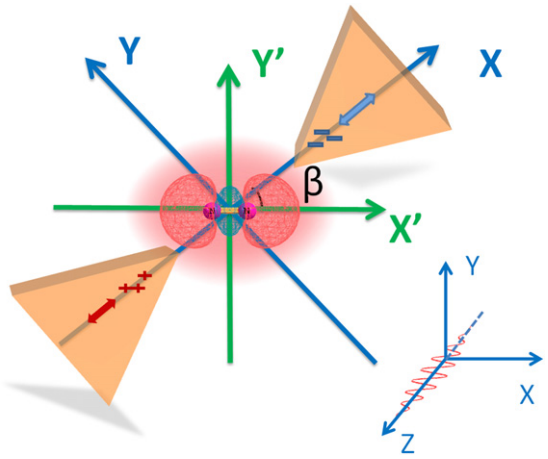

Figure 1. Schematic diagram of the initial state of N_2. (x, y, z) is the laboratory coordinate system, and (x', y', z') is the molecular coordinate system. The polarization direction of the incident laser electric field is along the x-axis and the input laser propagates along the z-axis; it is enhanced after passing through the gold bow-tie nanostructure then interacts with N_2 molecules radiating the harmonics. β is the angle between the x-axis and the x'-axis.

the HHG. When a gas of target molecules is injected into the small gap between the tips of the gold bow-tie shaped nanostructure, the incident laser which is enhanced after passing through the gap interacts with the symmetry molecules and the HHG is efficiently generated between the vertices of the nanostructure [50].

Before investigating the properties of generated high harmonics, we would like to make a few comments about high harmonic generation in inhomogeneous laser fields. Plasma-enhanced inhomogeneous laser fields can dramatically manipulate electron dynamics during the HHG process. Such inhomogeneous spatial distributions, as well as the observation of plasmonic HHG, were experimentally achieved in 2008 by exploiting the local fields enhancement induced by resonant plasmons within a metallic nanostructure consisting of bow-tie-shaped gold elements [29]. However, it has been under intense scrutiny recently. Sivis *et al* [58] conducted very similar experiments to those presented in [29]. In their experiments, all prominent features are attributed to atomic line emission (ALE) of neutral and ionized argon, and any signature of HHG has not been observed. This is a striking result. Later, Kim *et al* responsed to the scrutiny and stated that the two distinct phenomena, ALE and HHG, are not mutually exclusive but coexistent when gaseous atoms are illuminated by strong-field laser pulses. In their reply [59], Kim *et al* explained that the durability problem of the nanostructures may be the main reason for there having been no experimental demonstration of HHG from bow-ties in other groups. Furthermore, they concluded that bow-tie-shaped nanostructures might not be ideal for efficient HHG but tapered nanocones are a good alternative. The topic is still attractive and worth studying, since it enables one to elucidate some interesting physics. Many theoretical studies have already proved the feasibility of nanostructure-enhanced

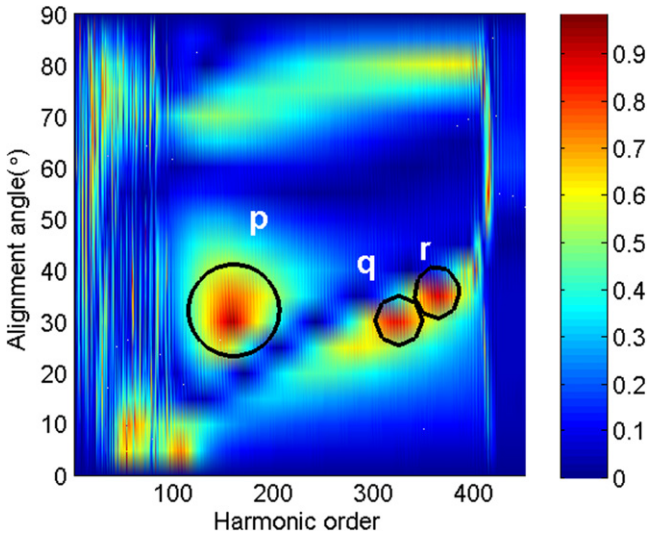

Figure 2. The harmonic ellipticity for different harmonic orders and alignment angles of N_2 molecule.

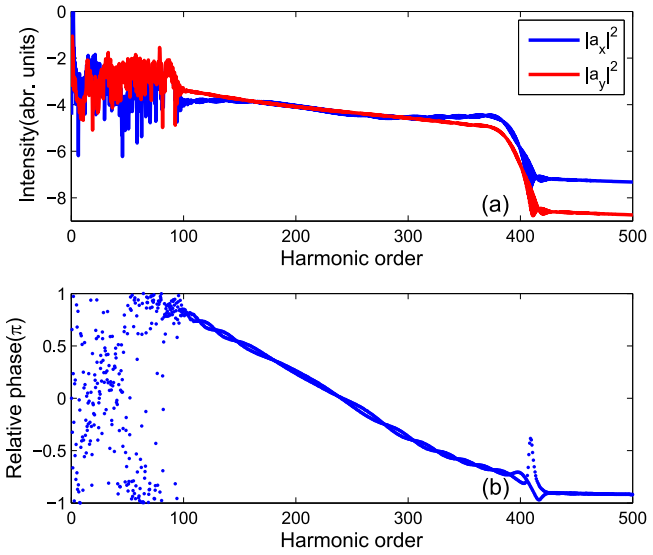

Figure 3. (a) The harmonic spectra along the x (blue curve) and y (red curve) directions in spatially inhomogeneous laser fields and (b) the relative phase of the two orthogonal harmonic components. Details of the laser parameters can be found in the main text.

HHG. Moreover, nanostructure-enhanced HHG has found many new application features [60, 61].

3.1. Near-circularly polarized attosecond laser pulse generation

In the following, to describe the polarization properties of the emitted harmonic spectra and generated attosecond pulses using the linearly polarized spatial inhomogeneous laser field, the ellipticity of the harmonics as a function of harmonic order and alignment angle is calculated according to equation (13). In this section, we chose $\kappa = 0.005$ and CEP $= 0$ to demonstrate the generation of the isolated near-circularly polarized attosecond laser pulse and plot the ellipticity spectrum in figure 2 for different harmonic orders and alignment angles. We change the alignment angle from 0° to 90° with a step of 5°. By comparing these results, we can find an appropriate angle to satisfy the best conditions for generating a near-circularly polarized attosecond pulse. Under the 100th harmonic order, due to the modulation of the harmonics (see figure 3(a)), the broadband supercontinuum cannot be generated, which indicates that the near-circularly polarized isolated attosecond pulse cannot be obtained in this region. Between the 100th and 400th harmonic orders, although the supercontinuum is generated (which can also be seen in figure 3(a)), the synthesized attosecond pulses are not all circularly polarized. As shown in figure 2, in the region of the 100th–400th harmonic orders, there are three main ellipticity peaks contributing to the near-circularly polarized pulse generation, marked by p, q, r. p is located at the alignment angle of 30° from the 140th to the 170th harmonic orders. The ellipticity is as large as 0.97, which supports the near-circularly polarized attosecond pulse generation. The other two peaks, q and r, whose ellipticity is a little smaller than peak p, can also support an isolated near-circularly polarized attosecond pulse generation. So in the following discussion, we take the peak p as an example to discuss the generation of the near-circularly polarized attosecond pulse corresponding to peak p.

Figure 3(a) shows the harmonic spectra along the x- and y- axes for the alignment angles of 30°. An important feature of the harmonic spectrum presented in figure 3(a) is the nonvanishing y component, which is perpendicular to the polarization direction of the driving laser field. It is shown that, under the 100th harmonic order in the first plateau of both x and y components, the harmonic spectrum has a strong modulation [6] due to the interference of the different recombination paths [2, 14]. Besides, for both the two components, the modulation disappears and the ultra-broadband supercontinuum is produced at the plateau from the 100th to about the 400th harmonic orders. It is worth mentioning that the broadband supercontinuum generation in figure 3(a) is attributed to the control of the quantum path by the spatial inhomogeneous driving field [47–50, 62] and the long wavelength driving laser. The synthesis of few-cycle pulses and spatially inhomogeneous electric fields has been proved to be capable of spatiotemporally manipulating the electron dynamics for broadband supercontinuum generation [63]. Due to the field inhomogeneity, the electrons that are released around the maximum of the driving field are further reaccelerated in the continuum and gain extra energy—compared with that in the homogeneous field—before recolliding with their parent ions [63]. This extra kinetic energy leads to a cutoff extension and also to a nice supercontinuum in the extended spectral region. It is well known that a broadband continuum can be generated if one of the electron trajectories (long or short path) that contributes to the harmonic generation is favored [2, 16]. We will show below that one of electron paths can be successfully selected due to the inhomogeneity of the driving laser field, which support the generation of isolated attosecond pulses with a duration of a few hundred attoseconds.

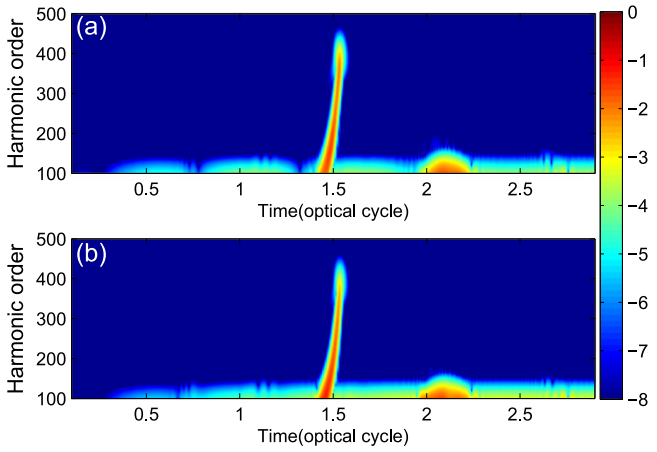

Figure 4. Time-frequency distribution of the HHG spectra along (a) the *x*-axis and (b) the *y*-axis corresponding to figure 2(a). The color scale is the same in this figure.

Comparing the two harmonic components, two characteristics are obvious from figure 3(a): one is that the supercontinuous spectra along the *x*- and *y*- axes have the same cutoff position and bandwidth. The other is that the intensities of the supercontinuous spectra along the *x*- and *y*- axes are comparable. Figure 3(b) shows the relative phase of the two components. From the 100th to the 400th harmonic orders, one can see that the relative phase of the two components is approximately a linear function of the harmonic orders. In the region of the 140th to 170th harmonic orders, the average value of the relative phase is $\frac{\pi}{2}$. These two features, i.e., the comparable intensity and near $\frac{\pi}{2}$ phase difference of the two harmonic components between the 140th and 170th, are inconsistent with the calculated ellipticity of the harmonics, which suggest that this part of harmonics can support a very short attosecond laser pulse with near-circular polarization.

To obtain a clear physical interpretation of the ultrabroadband supercontinuum, we perform a time-frequency analysis of the harmonic spectra [64]. Figures 4(a) and (b) present the time-frequency distributions of the harmonic spectra along the *x*- and *y*- axes for the alignment angle of 30°, corresponding to the harmonic spectrum of figure 3(a). The time-frequency distributions show that the two harmonic components emit at around 1.5 optical cycles, which indicates that the harmonic radiation of the two components are synchronous in the time domain and can support the synthesis of a circularly polarized laser pulse. The figure also reveals another feature; that there is only one harmonic radiation peak which appears around 1.5 optical cycles, which is different from the time-frequency distribution of harmonic spectra generated from the traditional spatial independence laser field. This feature can be attributed to the effect of the field inhomogeniety as well as the broken inversion symmetry [50]. The released electron experiences a quite different Lorentz force due to the spatial inhomogeneity of the electric field. Before the recombination with the parent ion, it acquires a larger kinetic energy [63], then very energetic photons can be emitted. Only one emission is synthesised by the 100th to 400th harmonic orders, which is consistent with the supercontinuous spectra in figure 3(a).

Next, we investigate the temporal characteristics of the circularly-polarized attosecond pulse generation. The temporal envelopes of the attosecond pulses of the two components are presented in figure 5. The attosecond pulses are synthesized from the 140th to 170th harmonic orders with the inhomogeneous driving field. The temporal profile of the attosecond pulse can be obtained by performing the inverse Fourier transformation in the selected spectrum region. In both components, we can intuitively see that the intensities of the two components are comparable. This figure clearly shows that only one pulse is generated due to the inhomogeneous laser field adopted, which is consistent with figures 4(a) and (b). The isolated pulse duration is approximately 155 as. The single attosecond pulses of the two components both occur at around 1.5 optical cycles, corresponding to the description in figure 4, which is conductive to the near-circularly polarized attosecond pulse generation.

In what follows, we further investigate the polarization feature of the generated near-circularly polarized isolated attosecond pulse. Figure 6(a) presents a 3D plot of the electric field of the generated isolated attosecond pulse for the alignment angle of 30° from the 140th to 170th harmonic orders. The projection of the electric field onto the time-E_x plane and the time-E_y plane are also presented. As shown in this figure, we can see that there is one pure attosecond pulse both for the *x* and *y* components and their electric fields are also comparable, corresponding to figures 3 and 5. The electric vector of the synthesized attosecond pulse rotates in the polarization plane, which indicates that the attosecond pulse is near-circularly polarized. Moreover, it can be judged for the emission time of the isolated attosecond pulses corresponding to figure 4. In order to clearly show the generation of a circularly polarized isolated attosecond pulse, the projection of the electric field onto the E_x-E_y plane is presented in figure 6(b). We calculate that the ratio between the largest and smallest field components of the ellipse in figure 6(b) is 1.06, which characterizes that the attosecond pulse obtained is near-circularly polarized. Besides region p shown in figure 2, the other supercontinuum regions with high ellipticity can also support an isolated near-circularly polarized attosecond laser pulse generation. The electric field of the generated isolated attosecond pulse for the region r at alignment 35° from the 350th to the 380th harmonic orders is also plotted in figures 6(c)–(d). The pulse duration is also 155 as, the same as for region p. So with the appropriate parameters, κ, CEP and wavelength, the isolated near-circularly polarized attosecond laser pulse with the same width pulse duration can be generated in the low-order range and high-order range simultaneously. Such a pulse may open additional avenues for applications in probing ultrafast electron dynamics.

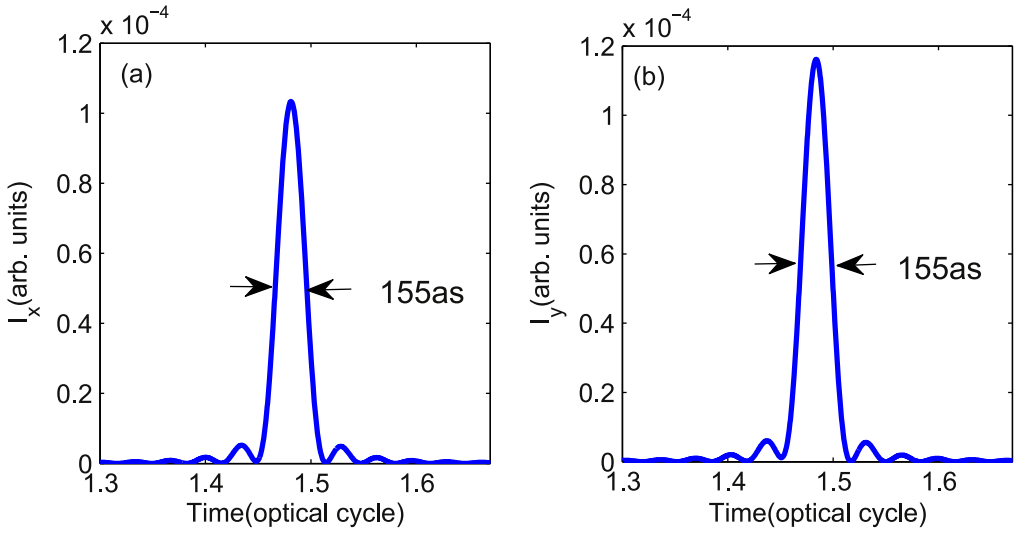

Figure 5. The attosecond pulse driving by the spatial inhomogeneous laser field from the 140th to the 170th harmonic orders along (a) the *x*-axis and (b) the *y*-axis. The FWHM of the two perpendicular components is 155 as.

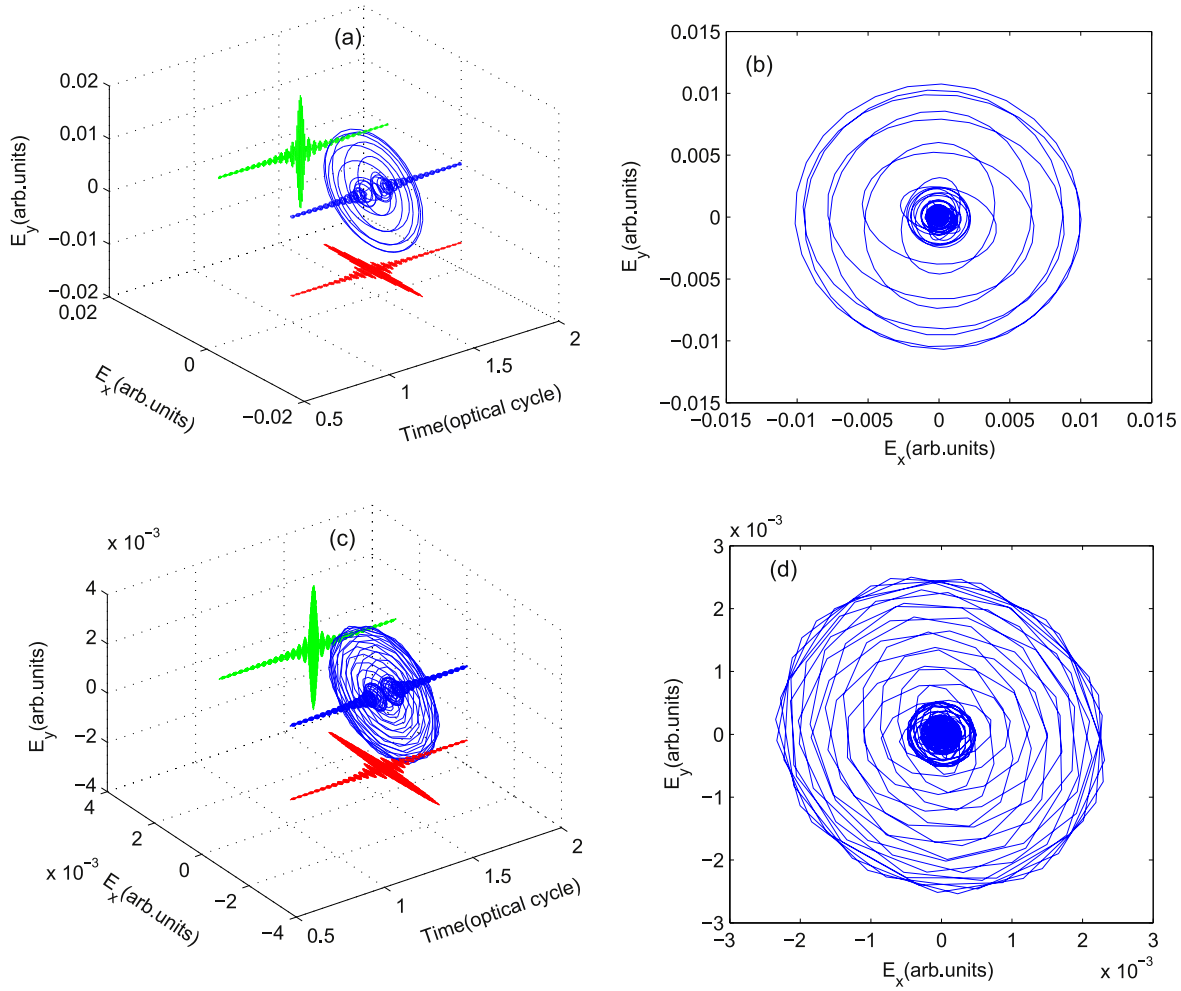

Figure 6. Nearly circularly polarized electric field of an attosecond pulse obtained by filtering the supercontinuum of the spectra shown in figure 3: (a) and (c) are the 3D temporal evolution of the electric fields at alignment angle 30° from the 140th to the 170th harmonic orders and at alignment angle 35° from the 350th to the 380th respectively. The red shadow represents the projection of the nearly polarized attosecond pulse on the *time*–E_x plane, as well as the green one on the *time*–E_y plane; (b) and (d) are projections of the electric field onto the E_x–E_y plane.

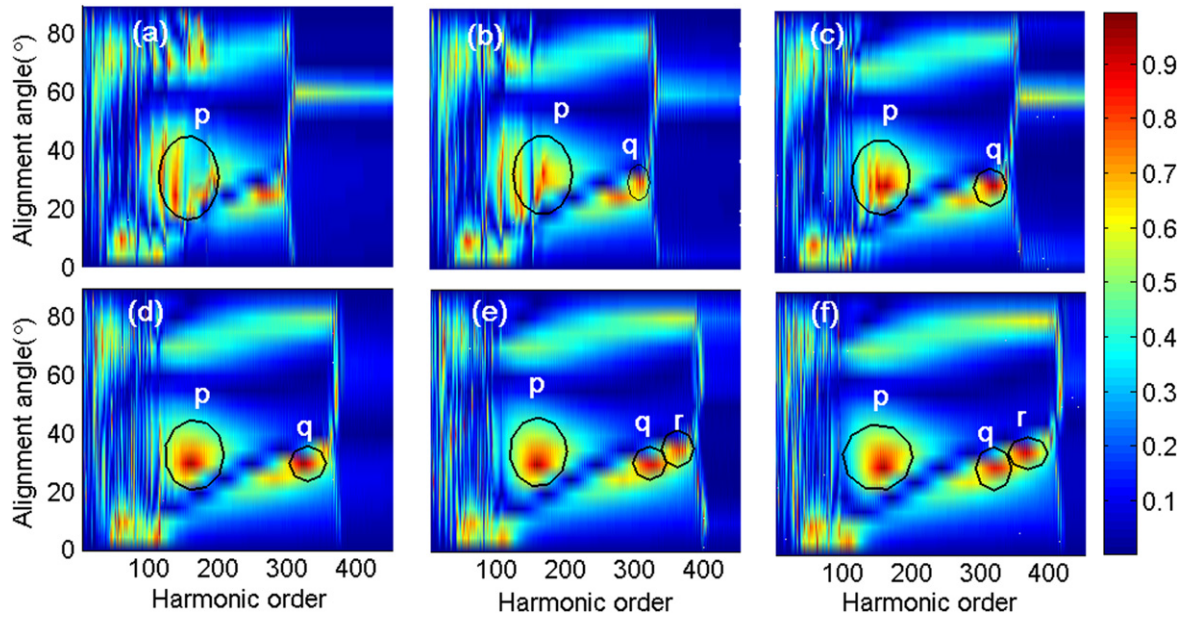

Figure 7. The harmonic ellipticity for different harmonic orders and alignment angles of N_2 molecule in the cases of (a) $\kappa = 0$, (b) $\kappa = 0.001$, (c) $\kappa = 0.002$, (d) $\kappa = 0.003$, (e) $\kappa = 0.004$, (f) $\kappa = 0.005$.

3.2. Role of the spatial inhomogeneity and the origin of the ellipticity

To make clear the role of the inhomogeneous field in the single near-circularly polarized attosecond laser pulse generation in our scheme, we calculated the ellipticity spectrum of the harmonics for different inhomogeneities, κ. For different $\kappa = 0$, 0.001, 0.002, 0.003, 0.004, 0.005 with CEP = 0, the results are exhibited in figure 7. In figure 7(a), when the driving laser field is spatially homogeneous ($\kappa = 0$), at the relative high ellipticity region marked as p located at the alignment angle of 30° from the 140th to the 170th harmonic order, there is a strong modulation so that no short single near-circularly polarized pulse can be generated. In figures 7(b)–(f), one can see that, with κ increased, the cutoff is extended and the supercontinuum becomes broader. Consequently, the spectra in region p become supercontiuum and regions q and r arise in the supercontinuum. All the results indicate that the field inhomogeneity plays a critical role in generating a single near-circularly polarized laser pulse both in the low-order range and the high-order range, due to its control of the quantum path of the electrons [28]. On the one hand, the inhomogeneous field is conductive to the generation of the broadband supercontinuum which ensures the generation of a short single near-circularly polarized isolated attosecond pulse. On the other hand, it extends the cutoff so that the single short near-circularly polarized isolated attosecond pulse can be generated in the extremely high frequency region. According to the analysis above, the spatial inhomogeneity influences the width of the supercontinuum and the cutoff position. However, the distribution of the harmonic ellipticity does not change, which indicates that the spatial inhomogeneity is not the origin of the ellipticity.

It is found in figure 7 that the distribution of the ellipticity map does not change with κ. This is also true for CEP (figure 8) and wavelength, as discussed below. All these results show that the harmonic ellipticity is not affected much by the laser parameters. They only influence the supercontinuum width and cutoff position. In fact, the ratio of the intensity and relative phase of the two harmonic components are determined by the feature of the recombination dipole of the rescattering wavepacket and the nonspherical molecular orbital [43], which is also shown in [43–46]. This means the ellipticity has a close relationship with the structure and alignment of the molecular orbital, and can be explained after calculating the recombination dipole moment. This point can also be confirmed by examining other molecules. We have stimulated this process by taking CO_2 as the target molecule. The parameters are the same as in section 3.1. Comparing the obtained ellipticity spectrum with that of the N_2 molecules of figure 2, the cutoff position and the width of the supercontinuum are almost the same. However, the ellipticity spectrum has a different structure. There are two ellipticity peaks which are located 60° from the 95th to the 105th harmonic order and 5° from the 320th to the 350th harmonic order, respectively. So, the result from the CO_2 also confirmed that the ellipticity has a close relationship with the structure and alignment of the molecule orbital. In addition, the result also shows that there is nothing special about N_2 molecules in the generation of the single near-circularly polarized attosecond laser pulse. Other molecules, i.e. CO_2, can also achieve our goal using our scheme.

3.3. Discussion on the laser parameters

For the short wavelengths of laser fields with durations of a few femtoseconds, the CEP of the laser field plays an important role in HHG. To check the stability of the scheme against CEP variation, we plotted the harmonic ellipticity in figure 8 for different harmonic orders and alignment angles in

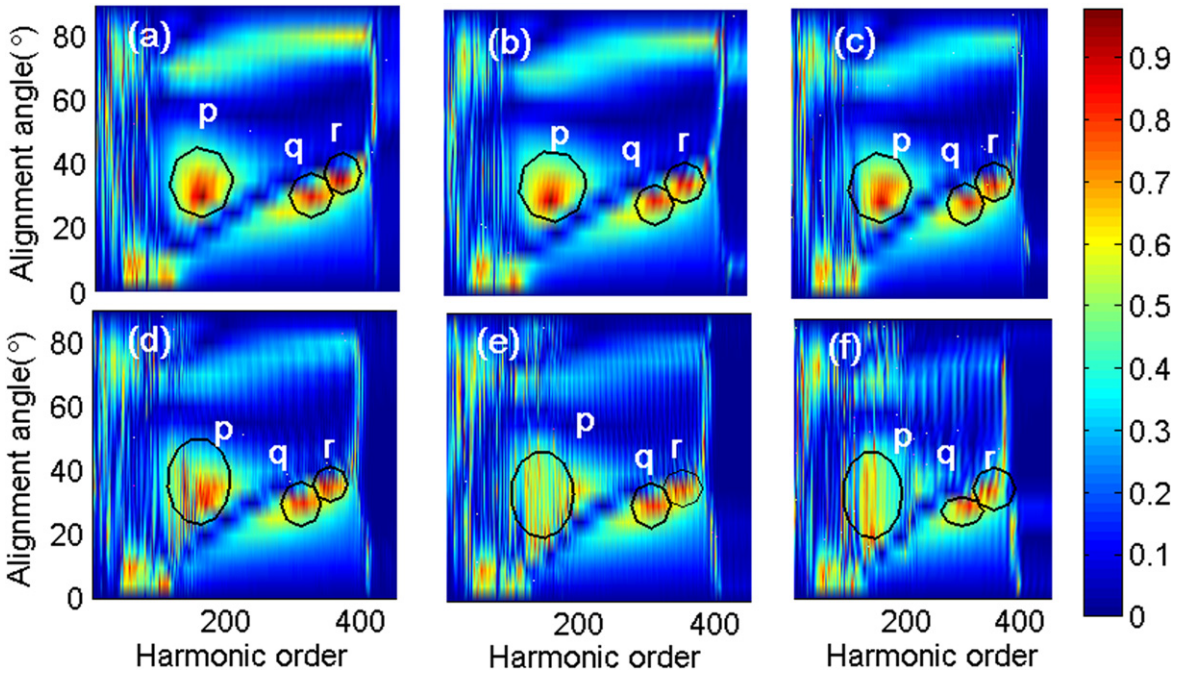

Figure 8. The harmonic ellipticity for different harmonic orders and alignment angles of N_2 molecule in the cases of (a) CEP = 0, (b) CEP = 0.1π, (c) CEP = 0.2π, (d) CEP = 0.3π, (e) CEP = 0.4π, (f) CEP = 0.5π.

the cases of CEP = 0, 0.1π, 0.2π, 0.3π, 0.4π, 0.5π. One can see that the distribution of the harmonic ellipticity does not change with CEP. However, the modulation in the harmonic spectra becomes more obvious and the bandwidth of the supercontinuum becomes narrower as the CEP increases. This can be associated with the interference of different recombination paths. The harmonic spectra in regions p, q, r of figures 8(a)–(c) are supercontinua. However, in figures 8(d)–(f), the region p has intense modulation, which means that an isolated pulse could not be generated in region p. But the regions q and r are still supercontinua. These results indicate that the generation of the isolated near-circularly polarized attosecond laser pulse for high harmonic orders (regions q, r) requires a CEP stability of less than that for low harmonic orders (region p), which is attributed to the role of the spatial inhomogeneous laser field [28]. So the optimized CEP is 0. If one wants to obtain the single near-circularly polarized laser pulse in the low-order range, the CEP can vary within 0–0.2 π. And if one wants to generate the pulse in the high-order range, the CEP can actually vary within a large range.

In the above calculation, we used the driving laser field of 1600 nm/6fs, which promises single near-circularly polarized laser pulse generation in both regions p and r. According to the CTSM, the use of long driving wavelength has been recognized as a promising route to cutoff extension and laser pulse generation at high harmonic orders because of $U_p \propto I\lambda^2$ where U_p is the ponderomotive energy of the electron in a laser field with intensity I and wavelength λ. In some experiments, it has been shown that a (sub)-two-cycle mid-IR laser pulse can be generated [65, 66]. But the generation of a near one-cycle mid-IR laser pulse demands very harsh experimental conditions. So we also stimulated the process by shortening the driving laser wavelength. We use 800 nm/3fs, which is produced easily in the experiment. It is found that the ellipticity distribution is the same as in figure 2 when we set the x-axis as the photon energy and an isolated near-circularly polarized laser pulse can also be generated in the region q. The region q in low-frequency harmonic orders does not change while the regions q and r in high-frequency orders disappear, as the cutoff is shortened by using the short wavelength of the laser field. This indicates that a few-cycle laser pulse at long wavelength is in favor of producing a high-frequency near-circularly polarized attosecond laser pulse. But if one only wants to obtain the low-frequency near-circularly polarized laser pulse, the requirement for the driving laser wavelength is absolutely relaxed. A short laser wavelength such as 800 nm can be used.

3.4. Alignment distribution

Next, considering the effect of imperfect alignment, we calculated the high-order harmonic spectrum generated from nonadiabatically aligned molecules. Here, an 800 nm, 100 fs alignment pulse with an intensity of 8.0×10^{13} W cm^{-2} is used. The rotational temperature is set to be 20 K. The HHG from alignment molecules is obtained by the coherent sum of the weighted $\rho(\theta, \tau)a_q(\omega)$, where $\rho(\theta, \tau)$ is the alignment distribution and θ is the angle between the molecular axis and the polarization of the probe pulse. More calculation details are shown in reference [67]. We plotted the ellipticity spectrum in figure 9(a) after considering alignment distribution. The y-axis is the alignment angle between the alignment laser field and the pump laser field which is used to generate the harmonics. From this figure, we can see that there are two ellipticity peaks located in the supercontinuum. We marked them as region p at alignment angle 35° from the 160th to the

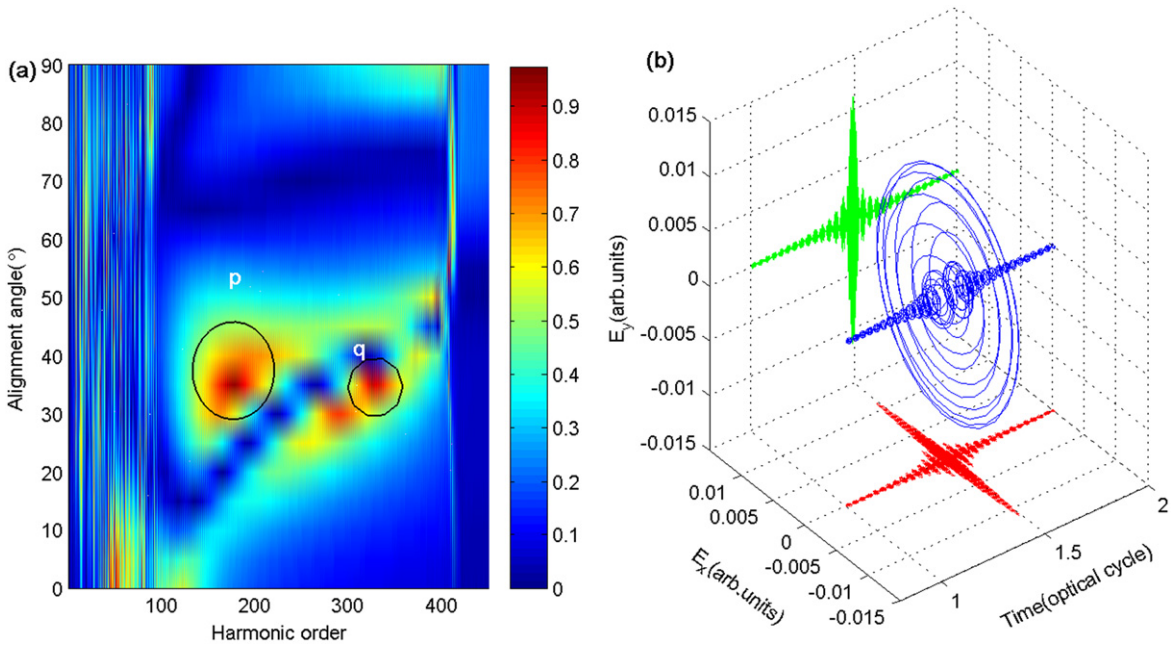

Figure 9. (a) The harmonic ellipticity for different harmonic orders and alignment angles of N_2 molecule after considering the alignment effect; (b) the 3D temporal evolution of the electric fields at alignment angle 35° from the 160th to the 190th harmonic order.

190th harmonic order and region q at alignment angle 35° from the 310th to the 340th harmonic order. The ellipticity peak q is 0.9, as high as p, which means that the near-circularly polarized attosecond laser pulse can be generated both in region p and q. Figure 9(b) shows the 3D plot of the electric field of the isolated attosecond pulse generated in region p. The pulse duration is 155 as. Comparing this figure with figure 2, the structure of the ellipticity spectrum does not change much except that the position for near-circularly polarized laser pulse generation is shifted about 5° upwards.

4. Conclusion

In summary, we have proposed a method for producing near-circularly polarized attosecond pulses in N_2 molecules using a linearly polarized driving laser field, which is enhanced by the metallic nanostructure. By changing the alignment angle between the spatially inhomogeneous driving laser linear polarization direction and the N_2 molecular axis, we have obtained multiple results regarding the ellipticity of the harmonics. We then get a largely elliptically polarized supercontinuum from the N_2 molecule at 30° alignment angle between the 140th to the 170th harmonic orders, which can support the isolated attosecond pulse generation with large ellipticity. The broadband supercontinuum generated is mainly attributed to the spatially inhomogeneous laser field. The intensities of the two components which polarize parallel and perpendicular to the driving laser polarization direction in the plane perpendicular to the propagation of the incident laser is comparable and the relative phase of the two components is about $\frac{\pi}{2}$. Therefore, the harmonics with these characteristics are in favor of the near-circularly polarized attosecond pulse generation with a duration of 155 as. We also calculate the ellipticity quantitatively, which provides guidance regarding the experimental generation of near-circularly polarized attosecond pulses.

Acknowledgments

This work was supported by the NNSF of China under grants no. 11404123, 11234004, and 61275126. Numerical simulations presented in this paper were carried out using the High Performance Computing Center experimental testbed in SCTS/CGCL (see http://grid.hust.edu.cn/hpcc).

References

[1] Paul P M, Toma E S, Breger P, Mullot G, Augé F, Balcou Ph, Muller H G and Agostini P 2001 Observation of a train of attosecond pulses from high harmonic generation *Science* **292** 1689–92
[2] Sansone G, Benedetti E, Calegari F, Vozzi C, Avaldi L, Flammini R, Poletto L, Villoresi P, Altucci C, Velotta R, Stagira S, De Silvestri S and Nisoli M 2006 Isolated single-cycle attosecond pulses *Science* **314** 443–6
[3] Chang Z, Rundquist A, Wang H, Murnane M M and Kapteyn H C 1997 Generation of coherent soft x rays at 2.7 nm using high harmonics *Phys. Rev. Lett.* **79** 2967
[4] Krausz F and Ivanov M 2009 Attosecond physics *Rev. Mod. Phys.* **81** 163–234
[5] Zhu X, Qin M, Li Y, Zhang Q, Xu Z and Lu P 2013 Tomographic reconstruction of molecular orbitals with twofold mirror antisymmetry: overcoming the nodal plane problem *Phys. Rev.* A **87** 045402
[6] Hentschel M, Kienberger R, Ch Spielmann, Reider G A, Milosevic N, Brabec T, Corkum P, Heinzmann U,

Drescher M and Krausz F 2001 Attosecond metrology *Nature* **414** 509–13
[7] Corkum P B and Krausz F 2007 Attosecond science *Nat. Phys.* **3** 381–7
[8] Zhu X, Qin M, Zhang Q, Li Y, Xu Z and Lu P 2013 Influence of large permanent dipoles on molecular orbital tomography *Opt. Express* **21** 5255–68
[9] Lein M 2007 Molecular imaging using recolliding electrons *J. Phys. B: At. Mol. Opt. Phys.* **40** 135–73
[10] Li Y, Zhu X, Lan P, Zhang Q, Qin M and Lu P 2014 Molecular-orbital tomography beyond the plane-wave approximation *Phys. Rev.* A **89** 045401
[11] Zhou Y, Huang C, Liao Q and Lu P 2012 Classical simula tions including electron correlations for sequential double ionization *Phys. Rev. Lett.* **109** 053004
[12] Dachraoui H, Michelswirth M, Siffalovic P, Bartz P, Schäfer C, Schnatwinkel B, Mattay J, Pfeiffer W, Drescher M and Heinzmann U 2011 Photoinduced reconfiguration cycle in a molecular adsorbate layer studied by femtosecond inner-shell photoelectron spectroscopy *Phys. Rev. Lett.* **106** 107401
[13] Drescher M, Hentschel M, Kienberger R, Uiberacker M, Yakovlev V, Scrinzi A, Th Westerwalbesloh, Kleineberg U, Heinzmann U and Krausz F 2002 Time-resolved atomic inner-shell spectroscopy *Nature* **419** 803–7
[14] Corkum P B 1993 Plasma perspective on strong field multiphoton ionization *Phys. Rev. Lett.* **71** 1994–7
[15] Christov I P, Murnane M M and Kapteyn H C 1997 High-harmonic generation of attosecond pulses in the 'single-cycle' regime *Phys. Rev. Lett.* **78** 1251
[16] Ferrari F, Calegari F, Lucchini M, Vozzi C, Stagira S, Sansone G and Nisoli M 2010 High-energy isolated attosecond pulses generated by above-saturation few-cycle fields *Nat. Photonics* **4** 875–9
[17] Lan P, Lu P, Cao W, Li Y and Wang X 2007 Isolated sub-100-as pulse generation via controlling electron dynamics *Phys. Rev.* A **76** 011402
[18] Chang Z 2004 Single attosecond pulse and xuv supercontinuum in the high-order harmonic plateau *Phys. Rev.* A **70** 043802
[19] Zhang Q, Lu P, Lan P, Hong W and Yang Z 2008 Multi-cycle laser-driven broadband supercontinuum with a modulated polarization gating *Opt. Express* **16** 9795–803
[20] Corkum P B, Burnett N H and Ivanov M Y 1994 Subfemtosecond pulses *Opt. Lett.* **19** 1870
[21] Sola I J, Mével E, Elouga L, Constant E, Strelkov V, Poletto L, Villoresi P, Benedetti E, Caumes J-P, Stagira S, Vozzi C, Sansone G and Nisoli M 2006 Controlling attosecond electron dynamics by phase-stabilized polarization gating *Nat. Phys.* **2** 319
[22] Takahashi E J, Lan P, Mücke O D, Nabekawa Y and Midorikawa K 2010 Infrared two-color multicycle laser field synthesis for generating an intense attosecond pulse *Phys. Rev. Lett.* **104** 233901
[23] Hong W, Lu P, Li Q and Zhang Q 2009 Broadband water window supercontinuum generation with a tailored mid-IR pulse in neutral media *Opt. Lett.* **34** 2102–4
[24] Lan P, Lu P, Li Q, Li F, Hong W and Zhang Q 2009 Macroscopic effects for quantum control of broadband isolated attosecond pulse generation with a two-color field *Phys. Rev.* A **79** 043413
[25] Pfeifer T, Gallmann L, Abel M, Neumark D and Leone S 2006 Single attosecond pulse generation in the multicycle-driver regime by adding a weak second-harmonic field *Opt. Lett.* **31** 975
[26] He L, Lan P, Zhang Q, Zhai C, Wang F, Shi W and Lu P 2015 Spectrally resolved spatiotemporal features of quantum paths in high-order-harmonic generation *Phys. Rev.* A **92** 043403
[27] Ciappina M F, Aćimović S S, Shaaran T, Biegert J, Quidant R and Lewenstein M 2012 Enhancement of high harmonic generation by confining electron motion in plasmonic nanostrutures *Opt. Express* **20** 26261
[28] Luo J, Li Y, Wang Z, Zhang Q and Lu P 2013 Ultra-short isolated attosecond emission in mid-infrared inhomogeneous fields without CEP stabilization *J. Phys. B: At. Mol. Opt. Phys.* **46** 145602
[29] Kim S, Jin J, Kim Y-J, Park I-Y, Kim Y and Kim S-W 2008 Highharmonic generation by resonant plasmon field enhancement *Nature* **453** 757–60
[30] Fetić B, Kalajdžić K and Milošević D B 2013 High-order harmonic generation by a spatially inhomogeneous field *Ann. Phys.* **525** 107
[31] Luo J, Li Y, Wang Z, He L, Zhang Q, Lan P and Lu P 2014 Efficient supercontinuum generation by UV-assisted midinfrared plasmonic fields *Phys. Rev.* A **89** 023405
[32] Sivis M, Duwe M, Abel B and Ropers C 2013 Extreme-ultraviolet light generation in plasmonic nanostructures *Nat. Phys.* **9** 304–9
[33] Ciappina M F, Shaaran T and Lewenstein M 2013 High order harmonic generation in noble gases using plasmonic fild enhancement *Ann. Phys.* **525** 97
[34] Mairesse Y, Higuet J, Dudovich N, Shafir D, Fabre B, Mével E, Constant E, Patchkovskii S, Walters Z, Yu Ivanov M and Smirnova O 2010 High harmonic spectroscopy of multichannel dynamics in strong-field ionization *Phys. Rev. Lett.* **104** 213601
[35] Yuan K J and Bandrauk A D 2012 Circularly polarized attosecond pulses from molecular high-order harmonic generation by ultrashort intense bichromatic circularly and linearly polarized laser pulses *J. Phys. B: At. Mol. Opt. Phys.* **45** 074001
[36] Stanciu C D, Hansteen F, Kimel A V, Kirilyuk A, Tsukamoto A, Itoh A and Rasing Th 2007 All-optical magnetic recording with circularly polarized light *Phys. Rev. Lett.* **99** 047601
[37] Xie X, Scrinzi A, Wickenhauser M, Baltuška A, Barth I and Kitzler M 2008 Internal momentum state mapping using high harmonic radiation *Phys. Rev. Lett.* **101** 033901
[38] Milošević D B, Becker W and Kopold R 2000 Generation of circularly polarized high-order harmonics by two-color coplanar field mixing *Phys. Rev.* A **61** 063403
[39] Kfir O, Grychtol P, Turgut E, Knut R, Zusin D, Popmintchev D, Popmintchev T, Nembach H, Shaw J M, Fleischer A, Kapteyn H, Murnane M and Cohen O 2014 Generation of bright phase-matched circularly polarized extreme ultraviolet high harmonics *Nat. Photonics* **9** 99
[40] Yuan K J and Bandrauk A D 2011 Circularly polarized molecular high-order harmonic generation in H_2^+ with intense laser pulses and static fields *Phys. Rev.* A **83** 063422
[41] Yuan K J and Bandrauk A D 2013 Single circularly polarized attosecond pulse generation by intense few cycle elliptically polarized laser pulses and terahertz fields from molecular media *Phys. Rev. Lett.* **110** 023003
[42] Li Y, Zhu X, Zhang Q, Qin M and Lu P 2013 Quantum-orbit analysis for yield and ellipticity of high order harmonic generation with elliptically polarized laser field *Opt. Express* **21** 4896–907
[43] Mairesse Y, Levesque J, Dudovich N, Corkum P B and Villeneuve D M 2008 High harmonic generation from aligned molecules–amplitude and polarization *J. Mod. Opt.* **55** 2591
[44] Lee G H, Kim I J, Park S B, Kim T K and Nam C H 2008 Measurement of the polarization of high-order harmonics from aligned N_2 molecules by spatial interferometry *Opt. Lett.* **33** 2083
[45] Zhou X, Lock R, Wagner N, Li W, Kapteyn H C and Murnane M M 2009 Elliptically polarized high-order

harmonic emission from molecules in linearly polarized laser fields *Phys. Rev. Lett.* **102** 073902
[46] Le A T, Lucchese R R and Lin C D 2010 Polarization and ellipticity of high-order harmonics from aligned molecules generated by linearly polarized intense laser pulses *Phys. Rev.* A **82** 023814
[47] Shaaran T, Ciappina M F, Guichard R, Pérez-Hernández J A, Roso L, Arnold M, Siegel T, Zaïr A and Lewenstein M 2013 High-order-harmonic generation by enhanced plasmonic near-fields in metal nanoparticles *Phys. Rev.* A **87** 041402
[48] Schuck P J, Fromm D P, Sundaramurthy A, Kino G S and Moerner W E 2005 Improving the mismatch between light and nanoscale objects with gold bowtie nanoantennas *Phys. Rev. Lett.* **94** 017402
[49] Park I-Y, Kim S, Choi J, Lee D-H, Kim Y-J, Kling M F, Stockman M I and Kim S-W 2011 Plasmonic generation of ultrashort extreme-ultraviolet light pulses *Nat. Photonics* **5** 677–81
[50] Yavuz I 2013 Gas population effects in harmonic emission by plasmonic fields *Phys. Rev.* A **87** 053815
[51] Feit M D, Fleck J A and Steiger A J R 1982 Solution of the Schrödinger equation by a spectral method *J. Comput. Phys.* **47** 412–33
[52] Peters M, Nguyen-Dang T, Charron E, Keller A and Atabek O 2012 Laser-induced electron diffraction: a tool for molecular orbital imaging *Phys. Rev.* A **85** 053417
[53] Shaaran T, Ciappina M F and Lewenstein M 2012 Quantum-orbit analysis of high-order-harmonic generation by resonant plasmon field enhancement *Phys. Rev.* A **86** 023408
[54] Krause J L, Schafer K J and Kulander K C 1992 Calculation of photoemission from atoms subject to intense laser fields *Phys. Rev.* A **45** 4998
[55] Zhu X, Qin M, Zhang Q, Hong W, Xu Z and Lu P 2012 Role of the Coulomb potential on the ellipticity in atomic high-order harmonics generation *Opt. Express* **20** 16275–84
[56] Pfullmann N, Waltermann C, Noack M, Rausch S, Nagy T, Reinhardt C, Kovačev M, Knittel V, Bratschitsch R, Akemeier D, Hütten A, Leitenstorfer A and Morgner U 2013 Bow-tie nano-antenna assisted generation of extreme ultraviolet radiation *New J. Phys.* **15** 093027
[57] Husakou A and Herrmann J 2014 Quasi-phase-matched high-harmonic generation in composites of metal nanoparticles and a noble gas *Phys. Rev.* A **90** 023831
[58] Sivis M, Duwe M, Abel B and Ropers C 2012 Nanostructure-enhanced atomic line emission *Nature* **485** E1
[59] Kim S, Jin J, Kim Y-J, Park I-Y, Kim Y and Kim S-W 2012 *Nature* Kim *et al* reply **485** E1–E3
[60] Feng L, Yuan M and Chu T 2013 Attosecond x-ray source generation from two-color polarized gating plasmonic field enhancement *Phys. Plasmas* **20** 122307
[61] Husakou A *et al* 2011 Polarization gating and circularly-polarized high harmonic generation using plasmonic enhancement in metal nanostructures *Opt. Express* **19** 25346
[62] Ciappina M F, Shaaran T, Guichard R, P erez-Hernández J A, Roso L, Arnold M, Siegel T, Zaïr A and Lewenstein M 2013 High energy photoelectron emission from gases using plasmonic enhanced near-fields *Laser Phys. Lett.* **10** 105302
[63] Yavuz I, Bleda E A, Altun Z and Topcu T 2012 Generation of a broadband xuv continuum in high-order-harmonic generation by spatially inhomogeneous fields *Phys. Rev.* A **85** 013416
[64] Antoine P, Piraux B and Maquet A 1995 Time profile of harmonics generated by a single atom in a strong electromagnetic field *Phys. Rev.* A **51** R1750
[65] Ishii N, Kaneshima K, Kitano K, Kanai T, Watanabe S and Itatani J 2014 Carrier-envelope phase-dependent high harmonic generation in the water window using few-cycle infrared pulses *Nat. Commun.* **5** 3331
[66] Shiner A D, Schmidt B E, Trallero-Herrero C, Wörner H J, Patchkovskii S, Corkum P B, Kieffer J-C, Légaré F and Villeneuve D M 2011 Probing collective multi-electron dynamics in xenon with high-harmonic spectroscopy *Nat. Phys.* **7** 464
[67] Qin M, Zhu X, Li Y, Zhang Q, Lan P and Lu P 2014 Probing rotational wave-packet dynamics with the structural minimum in high-order harmonic spectra *Opt. Express* **22** 6362